JACS
JOURNAL OF THE AMERICAN CHEMICAL SOCIETY
pubs.acs.org/JACS
Article

Nanoparticle-Catalyzed Green Chemistry Synthesis of Polybenzoxazole

Mengqi Shen, Chao Yu, Huanqin Guan, Xiang Dong, Cooro Harris, Zhen Xiao, Zhouyang Yin, Michelle Muzzio, Honghong Lin, Jerome R. Robinson, Vicki L. Colvin, and Shouheng Sun*

Cite This: J. Am. Chem. Soc. 2021, 143, 2115–2122
Read Online

ABSTRACT: Enabling catalysts to promote multistep chemical reactions in a tandem fashion is an exciting new direction for the green chemistry synthesis of materials. Nanoparticle (NP) catalysts are particularly well suited for tandem reactions due to the diverse surface-active sites they offer. Here, we report that AuPd alloy NPs, especially 3.7 nm $Au_{42}Pd_{58}$ NPs, catalyze one-pot reactions of formic acid, diisopropoxy-dinitrobenzene, and terephthalaldehyde, yielding a very pure thermoplastic rigid-rod polymer, polybenzoxazole (PBO), with a molecular weight that is tunable from 5.8 to 19.1 kDa. The PBO films are more resistant to hydrolysis and possess thermal and mechanical properties that are superior to those of commercial PBO, Zylon. Cu NPs are also active in catalyzing tandem reactions to form PBO when formic acid is replaced with ammonia borane. Our work demonstrates a general approach to the green chemistry synthesis of rigid-rod polymers as lightweight structural materials for broad thermomechanical applications.

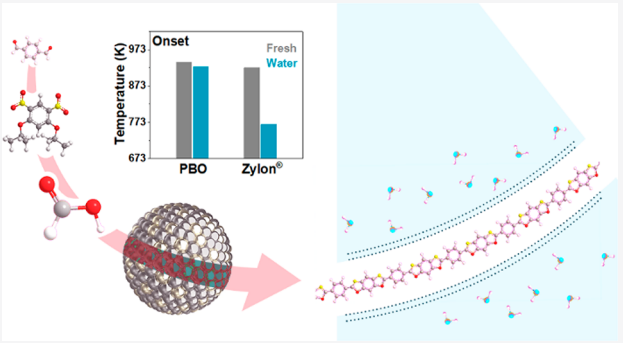

INTRODUCTION

Using nanoparticles (NPs) to integrate multiple chemical reactions is an exciting new direction for expanding the green chemistry synthesis of materials.[1−6] Recent advances in synthesis have allowed NPs to be made with precise control over their dimensions, structures, and compositions, which enables the rational tuning of NP catalysis to achieve higher reaction efficiencies under milder reaction conditions.[7−16] NP catalysts can also be designed to show more than one active surface site to promote multiple chemical reactions in a tandem fashion, which can greatly simplify the reaction systems and provide more efficient green chemistry approaches to material synthesis.[10,17−19]

While polymers are widely used to modify NP surface chemistry,[20−26] the potential for NPs to catalyze polymerization reactions has rarely been reported, most likely due to the NP surface deactivation caused by the strong polymer bonding. Recently, MPd NPs (M = Ag and Au) were studied to catalyze sequential formic acid dehydrogenation, nitroarene reduction, and aminoarene condensation with aldehydes to form benzoxazoles.[27,28] AuPd NP catalysis was extended to catalyze one-pot reactions of formic acid, 1,5-diisopropoxy-2,4-dinitrobenzene, and terephthalaldehyde for the formation of PBO.[28] However, the method achieved very low polymerization with molecular weights limited to 3.6 kDa.

Herein, we report a comprehensive study of NP-catalyzed one-pot reactions of formic acid, diisopropoxy-dinitrobenzene, and terephthalaldehyde (Scheme 1a−c) to form PBO (Scheme 1d) that is chemically stable for potential lightweight structural materials and thermomechanical applications.[29−31] We found that the first two reaction steps (Scheme 1a,b) were important to generating diaminobenzene for its next step reaction with terephthalaldehyde to form pre-PBO (Scheme 1c). Scheme 1c itself is an equilibrium reaction, and water must be removed to promote polymerization. Also, it is crucial to avoid early termination of the polymerization by the partial reduction product of nitro-amino-benzene (Scheme 1e). Studying the catalysis of different AuPd NPs (sizes of 3.7, 6.2, 8.5, and 10.5 nm; compositions $Au_{29}Pd_{71}$, $Au_{42}Pd_{58}$, $Au_{54}Pd_{46}$, and $Au_{65}Pd_{35}$), we found that 3.7 nm $Au_{42}Pd_{58}$ NPs were especially efficient at catalyzing the one-pot reactions for the formation of pre-PBO with tunable molecular weights (M_w) from 5.8 to 19.1 kDa. Pre-PBO could be converted to PBO via a simple thermal annealing process (Scheme 1d). The as-prepared 11.0 kDa PBO film showed significant thermal stability (up to 939 K) and a large tensile modulus (up to 11.4 GPa) comparable to that of commercial 40 kDa Zylon film (923 K and 12.1 GPa,

Received: November 30, 2020
Published: January 25, 2021

https://dx.doi.org/10.1021/jacs.0c12488
J. Am. Chem. Soc. 2021, 143, 2115−2122

Scheme 1. NP-catalyzed tandem reactions for the synthesis of PBO. (a) Dehydrogenation of formic acid to generate H_2. (b) Reduction of 1,5-diisopropoxy-2,4-dinitrobenzene with H_2 that is generated from a. (c) Condensation of 1,5-diisopropoxy-2,4-diaminobenzene (generated from b) and terephthalaldehyde to form pre-PBO. (d) Transformation of pre-PBO to PBO upon thermal annealing. (e) Side reaction that can lead to early termination of the polymerization by a half-reduction product, 2,4-diisopropoxy-5-nitroaniline.

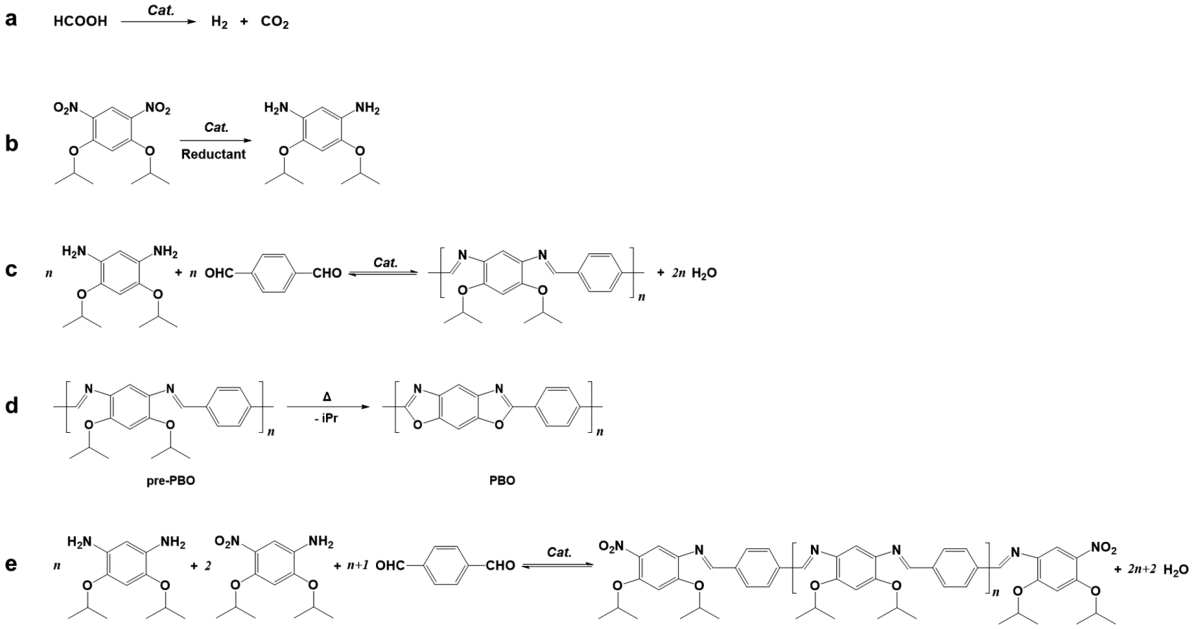

respectively). Most notably, the PBO film was much more stable against hydrolysis than commercial Zylon. After 1 week of immersion in boiling water (or a boiling aqueous solution of 0.5% phosphoric acid, PA), the 11.0 kDa PBO remained stable at temperatures of up to 926 K (or 865 K) and the film lost only 4% (or 24%) of its initial tensile modulus. After the same treatment, the commercial Zylon film decomposed at 767 K (or 710 K) and lost 53% (or 65%) of its tensile modulus. Similar reactions could also be catalyzed by 6.8 nm Cu NPs to form 9.5 kDa PBO when formic acid was replaced with ammonia borane. Our study offers a new NP-catalyzed green chemistry synthesis of rigid-rod polymers with high thermal and mechanical stability, which will be integral to applications as ballistic fibers, antiflame/heat-resistant coatings, and separation membranes.

RESULTS AND DISCUSSION

Synthesis of AuPd NPs. We modified the previously reported method to prepare AuPd NPs[32] and scaled up the synthesis of 3.7 nm AuPd NPs to the gram scale by the coreduction of $HAuCl_4$ and $Pd(acac)_2$ in oleylamine (Experimental Section). AuPd NP compositions ($Au_{29}Pd_{71}$, $Au_{42}Pd_{58}$, $Au_{54}Pd_{46}$, and $Au_{65}Pd_{35}$) were controlled by the molar ratio of $HAuCl_4/Pd(acac)_2$ and measured by inductively coupled plasma–atomic emission spectroscopy (ICP–AES) (Figures 1 and S1). AuPd NPs with different sizes (6.2, 8.5, and 10.5 nm) were synthesized by a seed-mediated growth method.[28] The as-prepared AuPd NPs were then supported on Ketjen carbon, and the surfactant was removed with acetic acid, yielding carbon (C)-supported NPs (Experimental Section). Figure 1a,b shows transmission electron microscopy (TEM) images of $Au_{42}Pd_{58}$ NPs and the $Au_{42}Pd_{58}$/C catalyst, respectively. $Au_{42}Pd_{58}$ NPs are monodisperse with a size of 3.7 ± 0.2 nm. A representative high-resolution TEM (HRTEM) image of $Au_{42}Pd_{58}$ (inset of Figure 1b) shows a clear (111) lattice fringe distance of 0.227 nm, which is between that of face-centered cubic (fcc) Au (0.235 nm) and fcc Pd (0.223 nm).[28] The uniform distribution of Au and Pd elements within one AuPd NP is revealed by high-angle annular dark field–scanning TEM (HAADF–STEM) and elemental mapping (Figure 1c). The fcc-type alloy structure of the AuPd NPs is further confirmed by X-ray diffraction (XRD), with their (111) peak shifts dependent on the Au/Pd alloy composition (Figure S2). Au (3.7 ± 0.3 nm) and Pd (4.4 ± 0.4 nm) NPs were also prepared (Figure S3)[33,34] and were used as controls.

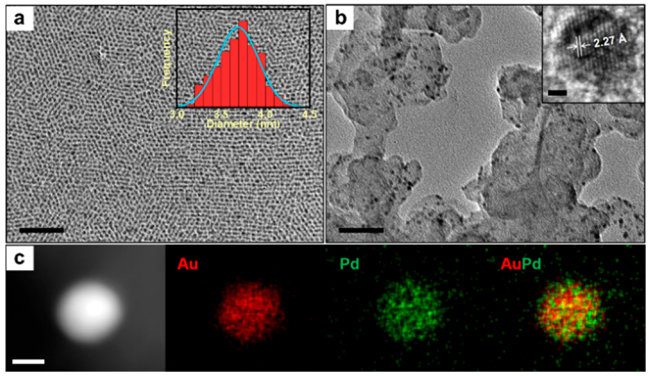

Figure 1. Characterization of 3.7 nm $Au_{42}Pd_{58}$ NPs. TEM images of (a) $Au_{42}Pd_{58}$ (inset: NP size distribution) and (b) $Au_{42}Pd_{58}$/C (inset: HRTEM), scale bar 50 nm (inset: 1 nm). (c) HAADF–STEM and elemental mapping of a representative $Au_{42}Pd_{58}$ NP, scale bar 2 nm.

AuPd NP Catalysis. We screened the NP-catalyzed reactions (Scheme 1a–c) and found that 3.7 nm $Au_{42}Pd_{58}$ NPs were much more active than Pd, Au, and other AuPd NPs. Here we used this 3.7 nm AuPd NP catalyst as an example to highlight its potential for enabling the green chemistry synthesis of PBO.

https://dx.doi.org/10.1021/jacs.0c12488
J. Am. Chem. Soc. 2021, 143, 2115–2122

Maximizing the reaction yield from each step (Scheme 1a–c) without early termination of the polymerization process (Scheme 1e) is critical to increasing the polymer length. We first studied formic acid dehydrogenation (Scheme 1a) catalyzed by 3.7 nm AuPd NPs in *N*-methyl-2-pyrrolidone (NMP), a solvent we used for all three step reactions (Scheme 1a–c). The AuPd alloy NPs were more active than the pure Au or Pd NPs (Figure 2a), and the $Au_{42}Pd_{58}$ NP catalyst has the highest turnover frequency (TOF) value of 235.5 h^{-1}, which is 4.2 times higher than that of pure Au (55.8 h^{-1}) and 3.1 times higher than that of pure Pd (76.2 h^{-1}) (Figure 2b). Temperature-dependent formic acid dehydrogenation gave an apparent reaction activation energy of 31.6 ± 1.5 kJ/mol (Figure S4a,b). Formic acid could be fully decomposed to H_2 and CO_2 by the $Au_{42}Pd_{58}$ NP catalyst within 2 h at 353 K.

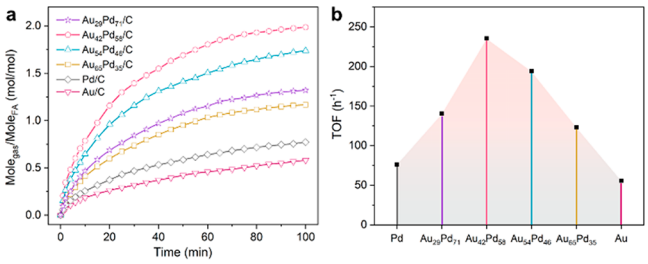

Figure 2. NP-catalyzed formic acid dehydrogenation. (a) Time-dependent molar ratios of the total gas (H_2 + CO_2) produced over the moles of formic acid present in the reaction solution. (b) TOF values normalized to the overall metal content (Au + Pd) for formic acid dehydrogenation by different catalysts. Reaction conditions: formic acid (10 mmol), AuPd/C catalysts (0.25 mol %), and NMP (3 mL) at 353 K.

Next, we coupled Scheme 1a,b to reduce 1,5-diisopropoxy-2,4-dinitrobenzene to evaluate the efficacy of the one-pot generation of 1,5-diisopropoxy-2,4-diaminobenzene. The buildup of excess CO_2 and H_2 from the reaction (Scheme 1a) was managed simply by attaching a balloon to the reaction vessel. The NO_2-reduction results are summarized in Figure 3a. The $Au_{42}Pd_{58}$ NP catalyst is also the most active for the tandem reactions, where the diamine product was produced in 95% yield after 2 h at 353 K. Achieving a high-yield full conversion of $-NO_2$ to $-NH_2$ is essential to the next step in the polymerization, as the partial hydrogenation product can also react with terephthalaldehyde, terminating the condensation polymerization reaction (Scheme 1e).

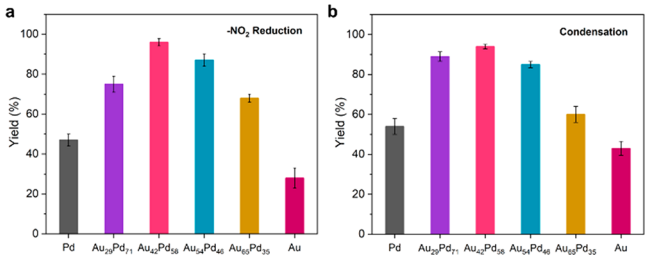

Figure 3. NP composition-dependent catalysis in the reduction and condensation reaction. (a) NP composition-dependent yields of 1,5-diisopropoxy-2,4-diaminobenzene produced by the NP-catalyzed reduction of 1,5-diisopropoxy-2,4-dinitrobenzene. Reaction conditions: AuPd/C catalysts (2.5 mol %), 1,5-diisopropoxy-2,4-dinitrobenzene (1 mmol), formic acid (10 mmol), and NMP (3 mL), 353 K, 2 h. (b) NP-composition-dependent yields of the Schiff-base products formed by the NP-catalyzed condensation of 1,5-diisopropoxy-2,4-diaminobenzene and benzaldehyde. Reaction conditions: AuPd/C catalysts (2.5 mol %), 1,5-diisopropoxy-2,4-diaminobenzene (1 mmol), benzaldehyde (2 mmol), NMP (3 mL), toluene (1 mL), 403 K, 6 h, Ar flow.

The diamine-dialdehyde condensation reaction is the critical propagation step in forming pre-PBO (Scheme 1c) and is an equilibrium reaction in which water must be removed in order to drive the reaction to completion. The isopropyl group is attached to the nitroarene to ensure the good solubility of pre-PBO in NMP. Using the condensation of 1,5-diisopropoxy-2,4-diaminobenzene and benzaldehyde as a model reaction (Figure S5), we studied the reaction with and without water removal. At 353 K with a balloon-sealed reaction vessel, the Schiff-base product was formed in 62% yield due to excess water being trapped in the reaction system (Figure S6). This yield could not be improved by increasing the reaction temperature due to the exothermic reaction nature of the condensation reaction. To remove water from the reaction system, we added toluene as a low-boiling azeotropic agent to facilitate water removal and let the reaction proceed under a gentle flow of Ar. Indeed, we saw a dramatic increase in the Schiff-base product yield with the increase of the reaction temperature (Figure S6), reaching 94% at 403 K. After studying AuPd composition-dependent catalysis on the condensation reaction at 403 K for 6 h, we concluded that the $Au_{42}Pd_{58}$ is still the best at catalyzing the reaction (Figure 3b). Another criterion to ensure an effective condensation reaction (Scheme 1c) is the complete consumption of all formic acid from previous reactions (Scheme 1a,b) before the Scheme 1c reaction is started. Otherwise, the extra formic acid could reduce −CHO to $-CH_3$ under the current catalytic condition (Figure S7), which is also common in the Pd-catalyzed deoxygenation of aldehyde to a methyl group, lowering the PBO formation yield.[35−38] Overreduction was avoided by performing the first two steps (Scheme 1a,b) at 353 K and carrying out the subsequent condensation polymerization at 403 K with the addition of aldehyde and toluene to the reaction mixture under a gentle flow of Ar (Figure S8). This furnished the Schiff-base product in greater than 90% yield.

One-Pot Synthesis of PBO. The conventional methods for preparing PBO require extremely corrosive and reactive chemicals,[30,31,39−41] which are the antithesis of those preferred in green chemistry. One common route is to polymerize 4,6-diamino resorcinol dihydrochloride and terephthalic acid with poly(phosphoric acid) (PPA) functioning as the solvent, catalyst, and dehydration agent.[30,31] The PBO prepared from this method is inevitably contaminated by PA units, which cannot be removed from the polymer structure. The presence of the PA units in the polymer structure is believed to be the main reason for the thermal and mechanical failures of Zylon in the presence of moisture due to PA-catalyzed Schiff-base bond hydrolysis.[42−44] Different from these previous organic reactions used to prepare PBO, our AuPd-catalyzed reactions require much less toxic and more stable chemicals, such as formic acid, nitroarene, and aldehyde, as precursors to preparing PBO. On the basis of what we concluded from studying the Scheme 1a–c reactions, we applied two temperature stages for polymerization: the first stage at 353 K to complete the reactions (Scheme 1a&b) in a balloon-sealed reaction system and the second stage at 403 K under a gentle flow of Ar with terephthalaldehyde and toluene added to

https://dx.doi.org/10.1021/jacs.0c12488
J. Am. Chem. Soc. 2021, 143, 2115−2122

remove water more efficiently and to complete the Scheme 1c reaction.

The Fourier transform infrared spectrum (FT-IR) of pre-PBO shows peaks of C═N (1618 cm^{-1}), C−N (1372 cm^{-1}), and C−O (1184, 1096 cm^{-1}) (Figure S9). Size-exclusion chromatography (SEC) was used to measure the molecular weight of pre-PBO. The degree of polymerization of pre-PBO was controlled from 5.8 to 11.0 kDa by adjusting the reaction time (Figure S10 and Table S1). After 6 h of reaction, the polymer stopped growing. This is very likely caused by the presence of a small amount (<5%) of a partial reduction intermediate, such as 2,4-diisopropoxy-5-nitroaniline, in the reaction mixture. This reaction byproduct can interfere with the condensation polymerization at a later stage. As the intended diamine reactant is consumed, this intermediate may condense with the aldehyde, thereby terminating the polymer growth. Using a simple concentration-dependent polymer growth model, we calculated that when there is 5% of the nitroaniline intermediate present in the reaction mixture, the theoretical molecular weight of the pre-PBO product would be ~12 kDa (Figure S11), which is consistent with what we obtained in our synthesis (11.0 kDa). Moreover, the M_w could be further increased to 19.1 kDa when we conducted the polymerization reaction (Scheme 1c) with pure 1,5-diisopropoxy-2,4-diaminobenzene (Figure S12).

PBO was prepared by heating pre-PBO, which removed isopropyl groups and triggered intramolecular cyclization to form benzoxazole rings (Scheme 1d). Dynamic thermal gravimetric analysis (TGA) of pre-PBO showed a significant weight drop at 623 K (Figure S13a). Static TGA at 623 K caused a quick mass drop in the sample to 73.1% of the original value, which is in agreement with the calculated weight retention at 72.7% after the total loss of the isopropyl group, indicating a full transformation from pre-PBO to PBO (Figure S13b). IR spectra of the PBO powder show the characteristic peaks of C═N (1615 cm^{-1}), C−N (1364 cm^{-1}), and C−O (1049 cm^{-1}), which agree well with those from Zylon (Figure S14a). UV−vis absorption and photoluminescence (PL) spectra of PBO and Zylon (Figure S14b,c) are almost identical, indicating that the PBO prepared from our catalysis reactions has the same highly conjugated aromatic structure as Zylon. ICP−AES analysis (detection limit <20 ppb) of the PBO product showed no detectable quantity of P elements, proving that the PBO we prepared is PA-free. Furthermore, we analyzed the $Au_{42}Pd_{58}$ catalyst stability before and after the polymerization reactions and found the catalyst to be very stable. TEM, X-ray photoelectron spectroscopy (XPS), ICP−AES, and the degree polymerization (Figure S15 and Table S2) all support that this catalyst is stable and reusable under the current reaction conditions. In all, the 3.7 nm $Au_{42}Pd_{58}$ NPs provide a novel, green, efficient catalysis approach to the one-pot synthesis of PA-free PBO.

PBO Property Studies. The application of Zylon is hindered by its poor long-term stability due to the unexpected hydrolysis-induced polymer structure degradation.[42−44] Zylon intrinsically contains 0.5% PA units in its polymer structure that cannot be removed via any purification process. In contrast, our PBO is PA-free, which enables us to study the impact of PA on the hydrolysis of the benzoxazole ring structure, which degrades the polymer. We prepared the 11.0 kDa PBO film (~10 μm thick) (Figure S16) and immersed the film in boiling water (or a boiling aqueous solution of 0.5% PA) for 1 week to study the effect of water (or PA) on PBO stability. A Zylon film was prepared similarly and treated in the same way for comparison. After washing and drying the films, we measured the thermal stability of these films with TGA under a N_2 atmosphere (Figure 4a,b). The onset decomposition temperatures of the pristine PBO and Zylon films were 939 and 923 K, respectively. After 1 week of exposure to boiling water or PA solution, the PBO film maintained a high onset decomposition temperature (H_2O, 926 K; PA, 865 K), while the onset decomposition temperature of the Zylon film decreased significantly (H_2O, 767 K; PA, 710 K). We further measured the mechanical stability of both films using the tensile stress test (Figure S17a,b). The gradient shadow in Figure 4c illustrates the difference in tensile strength retention between the PBO and Zylon films. The 11.0 kDa PBO film has an initial mechanical strength (50.2 MPa) that is comparable to that of the Zylon film (63.9 MPa). (The 19.1 kDa PBO has a strength value of 57.2 MPa (Figure S18).) After the H_2O (or PA) treatment, the 11.0 kDa PBO film retained its tensile strength to a much larger degree (H_2O, 42.5 MPa and 15% drop; PA, 32.1 MPa and 36% drop) than did the commercial Zylon film (H_2O, 24.8 MPa and 61% drop; PA, 12.7 MPa and 80% drop). The tensile modulus of the PBO film (11.4 GPa) was lowered to 10.9 GPa (H_2O) or 8.7 GPa (PA) after the treatment, while the value of the Zylon film (12.1 GPa) decreased to 5.7 GPa (H_2O) or 4.2 GPa (PA) (Figure 4d). The PBO we prepared has an even higher potential for showing long-term thermomechanical stability if it is made into fibers with mechanical alignment similar to that of Zylon fibers. Taken together, these clearly demonstrate that PBO made from our AuPd-catalyzed one-pot reactions is PA-free and is thermally, chemically, and mechanically much more robust than commercial Zylon.

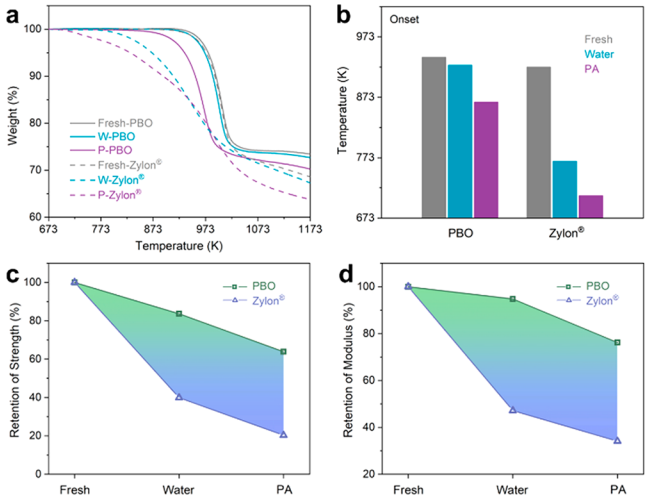

Figure 4. Stability tests of as-prepared PBO and commercial Zylon films. (a) Dynamic TGA curves of PBO and Zylon films after immersion in boiling water or PA for 1 week. (b) Onset decomposition temperatures of PBO and Zylon films after 1 week of boiling water or PA treatment. (c) Tensile strength retention and (d) tensile modulus retention of PBO and Zylon films before and after immersion in boiling water and PA solution for 1 week.

Extension of NP Catalysis for PBO Formation. We reasoned that the NP-catalyzed one-pot reaction approach to the synthesis of PBO could be extended to other types of NPs that are active in catalyzing tandem dehydrogenation and hydrogenation reactions. Among various earth-abundant metal

https://dx.doi.org/10.1021/jacs.0c12488
J. Am. Chem. Soc. 2021, 143, 2115−2122

NPs that have been synthesized, we selected Cu NPs to study their tandem catalysis.[10] Our preliminary studies showed that 6.8 nm Cu NPs (Figure S19) were not suitable for catalyzing formic acid dehydrogenation because they were not stable in the acidic solution. However, Cu NPs were found to be active in promoting the decomposition of ammonia borane to release H_2. More interestingly, these Cu NPs catalyzed one-pot reactions of ammonia borane, diisopropoxy-dinitrobenzene, and terephthalaldehyde to form very pure PBO (M_w = 9.5 kDa) (Figure S20). This suggests the great potential of extending NP catalysis to the green chemistry synthesis of PBO or other rigid-rod polymer materials.

CONCLUSIONS

NPs can catalyze a three-step process for forming very pure rigid-rod polymer PBO while utilizing more environmentally friendly solvents and biorenewable reactants than in the conventional route. Size- and composition-dependent AuPd catalysis studies show that 3.7 nm $Au_{42}Pd_{58}$ NPs are especially active and selective for catalyzing all three reactions in the formation of pre-PBO, yielding products of controllable M_w from 5.8 to 19.1 kDa. Pre-PBO is converted to PBO by a simple annealing process at 623 K. The as-synthesized PBO film is thermally stable at temperatures of up to 939 K and can withstand a mechanical strength of up to 57.2 MPa, properties comparable to those of a commercial Zylon film. After immersion in boiling water for 1 week, the PBO films showed a minimal thermal decomposition difference (from 939 to 923 K) with only a 15% decrease in mechanical strength. In comparison, the commercial Zylon films had a sharp decrease in thermal stability (from 923 K down to 767 K) and lost 61% of their mechanical strength. Our study demonstrates that, when prepared from NP-catalyzed green chemistry reactions, the resulting PBO films are more thermally, mechanically, and chemically robust than commercial Zylon, which suffers from unavoidable contamination with phosphoric acid. Moreover, this NP-catalyzed tandem reaction system for controlled polymerization can be extended to non-noble metal NPs such as Cu NPs, providing a general green and cost-effective approach to the preparation of PBOs or other rigid-rod polymers for ballistic fiber, antiflame/heat-resistant coating, and separation membrane applications.

EXPERIMENTAL SECTION

Chemicals and Materials. Palladium acetylacetonate ($Pd(acac)_2$, 99%) and hydrogen tetrachloroaurate hydrate ($HAuCl_4$, 99.8%) were purchased from Strem Chemicals. Oleylamine (OAm, technical grade, 70%), borane tert-butylamine (97%), 1,2,3,4-tetrahydronaphthalene (tetralin, 99%), formic acid (95%), 1,5-difluoro-2,4-dinitrobenzene (97%), *N*-methyl-2-pyrrolidone (99%), methanesulfonic acid (99%), and various benzaldehydes were purchased from Sigma-Aldrich. Borane morpholine (97%) was purchased from Alfa Aesar. 1,5-Diisopropoxy-2,4-dinitrobenzene was prepared as reported.[32] Hexane (98.5%), isopropanol (99.5%), ethanol (100%), and acetic acid (98%) were purchased from Fisher Scientific. The deionized (DI) water was obtained from a Millipore Autopure System.

Synthesis of NP Catalysts. AuPd NPs were synthesized by modifying a previously reported recipe[33] and by scaling up to the gram scale. In a typical synthesis of 3.7 nm-$Au_{42}Pd_{58}$ NPs, borane morpholine (3 g) was dissolved by stirring in OAm (150 mL) under an Ar atmosphere at 343 K. The solution of $HAuCl_4$ (2.4 mmol) and $Pd(acac)_2$ (3.6 mmol) in OAm (60 mL) was rapidly transferred to the stirred borane morpholine solution at 343 K. The temperature was increased to 493 K and maintained for 30 min. Once the solution cooled, room-temperature isopropanol (1500 mL) was added to the reaction solution to precipitate the NP product that was separated by centrifugation at 8500 rpm for 10 min. $Au_{42}Pd_{58}$ NPs were purified twice by redispersing in hexane and flocculating with ethanol and were precipitated by centrifugation (8500 rpm, 10 min). The obtained $Au_{42}Pd_{58}$ NPs were redispersed in hexane for further study.

In the synthesis, the Au/Pd composition ratios in AuPd NPs were controlled by adjusting the amount of the precursors accordingly.

To deposit the NPs on the carbon support for next-step catalysis studies, 0.9 g of Ketjen carbon was suspended in 600 mL of hexane and sonicated for 2 h, and then 0.3 g of AuPd NPs suspended in hexane was added to the carbon support suspension under sonication for 2 h. AuPd/C was separated by centrifugation, washed with ethanol three times, and dried under vacuum. Then the AuPd/C was mixed with 150 mL of acetic acid and heated to 343 K overnight to remove the OAm surfactant. After cooling to room temperature, acetic acid solution was decanted, and the solid AuPd/C sample was washed twice with pure ethanol and twice more with hexane/ethanol (v/v 1/9) before being dried in vacuum.

Cu NPs (6.8 nm) were synthesized and deposited on the carbon support as reported previously[10] for catalysis studies.

Catalysis of Formic Acid Dehydrogenation. Catalysts and NMP (3 mL) were first mixed and stirred in a two-necked reactor at 298 K. Then, the mixture was heated to 353 K, at which point formic acid (10 mmol) was injected into the reactor and the produced gas was collected with a gas buret filled with water connected to the reactor. The volume of the gas mixture that evolved was measured by recording the volume of water displaced.

PBO Synthesis. The AuPd/C catalyst (2.5 mol %) and 1,5-diisopropoxy-2,4-dinitrobenzene (1 mmol) were first mixed in NMP (3 mL) and transferred to a balloon-sealed two-necked flask under an Ar atmosphere. The mixture was heated to 353 K, and formic acid (10 mmol) was rapidly injected. The mixture was kept at 353 K for 2 h. The reaction system was then placed under a gentle flow of Ar, and terephthalaldehyde (1 mmol) and toluene (1 mL) were added. The reaction mixture was further heated to 403 K and kept for 6 h at 403 K. Once cooled to room temperature, the catalyst was filtered, and the solution was poured into methanol (100 mL) to precipitate the pre-PBO product, which was filtered, rinsed several times with methanol, and dried in air. ^{1}H NMR (400 MHz, dimethyl sulfoxide-d_6): δ (ppm) 6.37 (s, 1H, Ar−H), 6.04 (s, 1H, Ar−H), 4.15 (hept, J = 6.1 Hz, 2H, CH), 4.10 (s, 4H, NH_2), 1.18 (d, J = 6.1 Hz, 12H, CH_3). ^{13}C NMR (101 MHz, dimethyl sulfoxide-d_6): δ (ppm) 135.0, 134.4, 109.0, 102.3, 71.7, 22.2.

One gram of pre-PBO was annealed at 623 K under N_2 for 2 h to convert it to PBO.

Preparation of PBO/Zylon Films. PBO and Zylon were mixed with methanesulfonic acid in a glass vial at 353 K for 5 h to dissolve. The polymer solution was transferred in a Petri dish that was heated in an oil bath. After solvent evaporation at 353 K for 3 h and at 403 K for 3 h, the film was immersed in water to peel off from the glass substrate. The obtained film was washed with water and dried at 353 K under vacuum for 12 h for further tests.

Stability Tests of PBO and Zylon. The as-prepared PBO and Zylon films were immersed in boiling water or an aqueous solution of 0.5% phosphoric acid (PA) for 1 week. After cooling to room temperature, the films were washed with water and dried at 353 K for 24 h under vacuum to give water-PBO/Zylon and PA-PBO/Zylon for thermal and mechanical tests.

Characterization. Transmission electron microscopy (TEM) images were acquired from a Philips CM20 (200 kV). High-resolution TEM (HRTEM) images were recorded with a JEOL 2100F (200 kV). Samples for TEM and HRTEM analyses were prepared by depositing a single drop of a dilute NP dispersion/suspension on amorphous-carbon-coated copper grids. TEM with a field-emission electron source and STEM analyses were obtained on a Hitachi HD2700C (200 kV) with a probe aberration correction. X-ray diffraction (XRD) patterns were collected on a Bruker AXS D8-Advanced diffractometer with Cu Kα radiation (= 1.5406 Å). Inductively coupled plasma−atomic emission spectroscopy was carried out on a JY2000 Ultrace ICP−AES equipped with a JY-AS

https://dx.doi.org/10.1021/jacs.0c12488
J. Am. Chem. Soc. 2021, 143, 2115−2122

421 autosampler and 2400 g/mm holographic grating. X-ray photoelectron spectroscopy (XPS) measurements were taken on a Thermo Scientific K-Alpha+ instrument using Avantage software. Spectra were acquired using an aluminum anode (Al Kα = 1486.6 eV) operating with a spot size of 200 μm. Survey scans were recorded at a pass energy of 200 eV, and region scans were recorded at a pass energy of 20 eV. The analyses of organic products were carried out with GC−MS using an Agilent 6890 GC coupled to a 5973 mass spectrometer detector with a DB-5 (Agilent) fused silica capillary column (length × i.d. = 30 m × 0.25 mm, df = 0.25 μm) and helium as the carrier gas. The mass spectrometer was operated in electron impact mode at a 70 eV ionization energy. Mass spectrometric data were acquired and processed using the GC−MS data system (Agilent Chemstation), and compounds were identified by comparing their gas chromatographic retention index and mass spectrum with those of authentic standards, the literature, and library data. The NMR characterization was carried out on a Bruker DRX (^{1}H, 400 MHz; ^{13}C, 101 MHz). The ^{1}H and ^{13}C NMR shifts are referenced relative to the solvent signal (DMSO; ^{1}H, 2.50 ppm; ^{13}C, 39.52 ppm). UV−vis absorption spectra were measured using a Cary 60 UV−vis spectrometer (Agilent Technologies) with a xenon flash lamp as the light source. Samples were dissolved in methanesulfonic acid (MSA) for the measurements. The solution photoluminescence measurements were performed on a FluoroMax-4 spectrofluorometer with a xenon arc lamp. Samples were dissolved in MSA for measurements. The excitation wavelength was 365 nm. Size-exclusion chromatography was performed using an Agilent 1260 equipped with two Poroshell 120 EC-C18 columns heated to 35 °C (4.6 × 100 mm^2, 2.7 μm) and a UV−vis diode array detector and a refractive detector. The eluant was inhibitor-free THF, and the system was calibrated with standard polystyrene standards ranging from 0.58 to 1500 kDa. The thermal stability was measured with a TGA/DSC 1 STARe System from Mettler Toledo provided with a horizontal balance. Approximately 5 mg of sample was placed in an aluminum pan and heated under an 80 mL/min nitrogen purge at a heating rate of 10 K/min. The change in weight was continuously registered. The mechanical properties of sample films were tested with a constant span length of 5 cm using upper/lower grips (Instron 2714-006) on an Instron 5942 load frame. A load was applied by moving the crosshead at a rate of 0.2 mm/min while measuring the force with a 500 N load cell (Instron 2580-105).

■ ASSOCIATED CONTENT

Supporting Information

The Supporting Information is available free of charge at https://pubs.acs.org/doi/10.1021/jacs.0c12488.

TEM images; formic acid dehydrogenation; model Schiff-base condensation reaction; condensation of 1,5-diisopropoxy-2,4-diaminobenzene and benzaldehyde; deoxygenation of benzaldehyde; AuPd NP-catalyzed tandem reactions; FT-IR spectrum of pre-PBO; pre-PBO characterization; theoretical molecular weight of pre-PBO; catalyzed condensation curves; thermotransformation of pre-PBO to PBO; spectroscopic characterization of as-prepared PBO and Zylon; recycling test of the $Au_{42}Pd_{58}$/C catalyst; as-prepared PBO film and the customized film cutter; stability of PBO mechanical properties; tensile strength test of as-prepared PBO films; Cu-catalyzed one-pot synthesis of pre-PBO; and NMR spectra and analytical data of compounds (PDF)

■ AUTHOR INFORMATION

Corresponding Author

Shouheng Sun − *Department of Chemistry, Brown University, Providence, Rhode Island 02912, United States;* orcid.org/0000-0002-4051-0430; Email: ssun@brown.edu

Authors

Mengqi Shen − *Department of Chemistry, Brown University, Providence, Rhode Island 02912, United States;* orcid.org/0000-0001-9265-6784

Chao Yu − *Department of Environmental and Chemical Engineering, Jiangsu University of Science and Technology, Zhenjiang, Jiangsu Province 212003, P. R. China;* orcid.org/0000-0002-4028-4250

Huanqin Guan − *Department of Chemistry, Brown University, Providence, Rhode Island 02912, United States*

Xiang Dong − *Department of Chemistry, Brown University, Providence, Rhode Island 02912, United States*

Cooro Harris − *Department of Chemistry, Brown University, Providence, Rhode Island 02912, United States*

Zhen Xiao − *Department of Chemistry, Brown University, Providence, Rhode Island 02912, United States;* orcid.org/0000-0002-3740-3546

Zhouyang Yin − *Department of Chemistry, Brown University, Providence, Rhode Island 02912, United States*

Michelle Muzzio − *Department of Chemistry, Brown University, Providence, Rhode Island 02912, United States*

Honghong Lin − *Department of Chemistry, Brown University, Providence, Rhode Island 02912, United States*

Jerome R. Robinson − *Department of Chemistry, Brown University, Providence, Rhode Island 02912, United States;* orcid.org/0000-0002-9111-3822

Vicki L. Colvin − *Department of Chemistry, Brown University, Providence, Rhode Island 02912, United States;* orcid.org/0000-0002-8526-515X

Complete contact information is available at: https://pubs.acs.org/10.1021/jacs.0c12488

Notes

The authors declare no competing financial interest.

■ ACKNOWLEDGMENTS

This work was supported in part by the Office of Vice President of Research of Brown University and the Institute of Molecular and Nanoscale Innovation of Brown University. M.M. was supported by a National Science Foundation Graduate Research Fellowship under grant no. 1644760. Zylon was generously supplied by Toyobo (USA) Inc.

■ REFERENCES

(1) Moreno-Mañas, M.; Pleixats, R. Formation of Carbon−Carbon Bonds Under Catalysis by Transition-Metal Nanoparticles. *Acc. Chem. Res.* **2003**, *36* (8), 638−643.

(2) Astruc, D.; Lu, F.; Aranzaes, J. R. Nanoparticles as Recyclable Catalysts: the Frontier Between Homogeneous and Heterogeneous Catalysis. *Angew. Chem., Int. Ed.* **2005**, *44* (48), 7852−7872.

(3) Turner, M.; Golovko, V. B.; Vaughan, O. P. H.; Abdulkin, P.; Berenguer-Murcia, A.; Tikhov, M. S.; Johnson, B. F. G.; Lambert, R. M. Selective Oxidation with Dioxygen by Gold Nanoparticle Catalysts Derived from 55-Atom Clusters. *Nature* **2008**, *454* (7207), 981−983.

(4) Kim, K.; Jung, Y.; Lee, S.; Kim, M.; Shin, D.; Byun, H.; Cho, S. J.; Song, H.; Kim, H. Directed C−H Activation and Tandem Cross-Coupling Reactions Using Palladium Nanocatalysts with Controlled Oxidation. *Angew. Chem., Int. Ed.* **2017**, *56* (24), 6952−6956.

(5) Muzzio, M.; Li, J.; Yin, Z.; Delahunty, I. M.; Xie, J.; Sun, S. Monodisperse Nanoparticles for Catalysis and Nanomedicine. *Nanoscale* **2019**, *11* (41), 18946−18967.

(6) Yin, Z.; Pang, H.; Guo, X.; Lin, H.; Muzzio, M.; Shen, M.; Wei, K.; Yu, C.; Williard, P.; Sun, S. CuPd Nanoparticles as a Robust Catalyst for Electrochemical Allylic Alkylation. *Angew. Chem., Int. Ed.* **2020**, *59*, 15933−15936.
(7) Hughes, M. D.; Xu, Y.-J.; Jenkins, P.; McMorn, P.; Landon, P.; Enache, D. I.; Carley, A. F.; Attard, G. A.; Hutchings, G. J.; King, F.; Stitt, E. H.; Johnston, P.; Griffin, K.; Kiely, C. J. Tunable Gold Catalysts for Selective Hydrocarbon Oxidation under Mild Conditions. *Nature* **2005**, *437* (7062), 1132−1135.
(8) Xie, X.; Li, Y.; Liu, Z.-Q.; Haruta, M.; Shen, W. Low-temperature Oxidation of CO Catalysed by Co_3O_4 nanorods. *Nature* **2009**, *458* (7239), 746−749.
(9) Zaera, F. Nanostructured Materials for Applications in Heterogeneous Catalysis. *Chem. Soc. Rev.* **2013**, *42* (7), 2746−2762.
(10) Shen, M.; Liu, H.; Yu, C.; Yin, Z.; Muzzio, M.; Li, J.; Xi, Z.; Yu, Y.; Sun, S. Room-Temperature Chemoselective Reduction of 3-Nitrostyrene to 3-Vinylaniline by Ammonia Borane over Cu Nanoparticles. *J. Am. Chem. Soc.* **2018**, *140* (48), 16460−16463.
(11) Muzzio, M.; Yu, C.; Lin, H.; Yom, T.; Boga, D. A.; Xi, Z.; Li, N.; Yin, Z.; Li, J.; Dunn, J. A.; Sun, S. Reductive Amination of Ethyl Levulinate to Pyrrolidones over AuPd Nanoparticles at Ambient Hydrogen Pressure. *Green Chem.* **2019**, *21* (8), 1895−1899.
(12) Cao, S.; Zhao, Y.; Lee, S.; Yang, S.; Liu, J.; Giannakakis, G.; Li, M.; Ouyang, M.; Wang, D.; Sykes, E. C. H.; Flytzani-Stephanopoulos, M. High-Loading Single Pt Atom Sites [Pt-O$(OH)_x$] Catalyze the CO PROX Reaction with High Activity and Selectivity at Mild Conditions. *Sci. Adv.* **2020**, *6* (25), eaba3809.
(13) Han, A.; Zhang, J.; Sun, W.; Chen, W.; Zhang, S.; Han, Y.; Feng, Q.; Zheng, L.; Gu, L.; Chen, C.; Peng, Q.; Wang, D.; Li, Y. Isolating Contiguous Pt Atoms and Forming Pt-Zn Intermetallic Nanoparticles to Regulate Selectivity in 4-Nitrophenylacetylene Hydrogenation. *Nat. Commun.* **2019**, *10* (1), 3787.
(14) Kuai, L.; Chen, Z.; Liu, S.; Kan, E.; Yu, N.; Ren, Y.; Fang, C.; Li, X.; Li, Y.; Geng, B. Titania Supported Synergistic Palladium Single Atoms and Nanoparticles for Room Temperature Ketone and Aldehydes Hydrogenation. *Nat. Commun.* **2020**, *11* (1), 48.
(15) Ryoo, R.; Kim, J.; Jo, C.; Han, S. W.; Kim, J.-C.; Park, H.; Han, J.; Shin, H. S.; Shin, J. W. Rare-Earth−Platinum Alloy Nanoparticles in Mesoporous Zeolite for Catalysis. *Nature* **2020**, *585* (7824), 221−224.
(16) Cui, X.; Huang, Z.; Van Muyden, A. P.; Fei, Z.; Wang, T.; Dyson, P. J. Acceptorless Dehydrogenation and Hydrogenation of N- and O-Containing Compounds on Pd_3Au_1(111) Facets. *Sci. Adv.* **2020**, *6* (27), eabb3831.
(17) Lee, J. M.; Na, Y.; Han, H.; Chang, S. Cooperative Multi-catalyst Systems for One-Pot Organic Transformations. *Chem. Soc. Rev.* **2004**, *33* (5), 302−312.
(18) Wasilke, J.-C.; Obrey, S. J.; Baker, R. T.; Bazan, G. C. Concurrent Tandem Catalysis. *Chem. Rev.* **2005**, *105* (3), 1001−1020.
(19) Yu, C.; Guo, X.; Shen, M.; Shen, B.; Muzzio, M.; Yin, Z.; Li, Q.; Xi, Z.; Li, J.; Seto, C. T.; Sun, S. Maximizing the Catalytic Activity of Nanoparticles through Monolayer Assembly on Nitrogen-Doped Graphene. *Angew. Chem., Int. Ed.* **2018**, *57* (2), 451−455.
(20) Xie, Y.; Qiao, Z.; Chen, M.; Liu, X.; Qian, Y. γ-Irradiation Route to Semiconductor/Polymer Nanocable Fabrication. *Adv. Mater.* **1999**, *11*, 1512−1515.
(21) Yavuz, M. S.; Cheng, Y.; Chen, J.; Cobley, C. M.; Zhang, Q.; Rycenga, M.; Xie, J.; Kim, C.; Song, K. H.; Schwartz, A. G.; Wang, L. V.; Xia, Y. Gold Nanocages Covered by Smart Polymers for Controlled Release with Near-Infrared Light. *Nat. Mater.* **2009**, *8* (12), 935−939.
(22) Akcora, P.; Liu, H.; Kumar, S. K.; Moll, J.; Li, Y.; Benicewicz, B. C.; Schadler, L. S.; Acehan, D.; Panagiotopoulos, A. Z.; Pryamitsyn, V.; Ganesan, V.; Ilavsky, J.; Thiyagarajan, P.; Colby, R. H.; Douglas, J. F. Anisotropic Self-Assembly of Spherical Polymer-Grafted Nanoparticles. *Nat. Mater.* **2009**, *8* (4), 354−359.
(23) Kango, S.; Kalia, S.; Celli, A.; Njuguna, J.; Habibi, Y.; Kumar, R. Surface Modification of Inorganic Nanoparticles for Development of Organic−Inorganic Nanocomposites—A review. *Prog. Polym. Sci.* **2013**, *38* (8), 1232−1261.
(24) Francis, R.; Joy, N.; Aparna, E. P.; Vijayan, R. Polymer Grafted Inorganic Nanoparticles, Preparation, Properties, and Applications: A Review. *Polym. Rev.* **2014**, *54* (2), 268−347.
(25) Zhang, M.; Wang, Y.-G.; Chen, W.; Dong, J.; Zheng, L.; Luo, J.; Wan, J.; Tian, S.; Cheong, W.-C.; Wang, D.; Li, Y. Metal (Hydr)oxides@Polymer Core−Shell Strategy to Metal Single-Atom Materials. *J. Am. Chem. Soc.* **2017**, *139* (32), 10976−10979.
(26) Han, A.; Chen, W.; Zhang, S.; Zhang, M.; Han, Y.; Zhang, J.; Ji, S.; Zheng, L.; Wang, Y.; Gu, L.; Chen, C.; Peng, Q.; Wang, D.; Li, Y. A Polymer Encapsulation Strategy to Synthesize Porous Nitrogen-Doped Carbon-Nanosphere-Supported Metal Isolated-Single-Atomic-Site Catalysts. *Adv. Mater.* **2018**, *30* (15), 1706508.
(27) Yu, C.; Guo, X.; Xi, Z.; Muzzio, M.; Yin, Z.; Shen, B.; Li, J.; Seto, C. T.; Sun, S. AgPd Nanoparticles Deposited on $WO_{2.72}$ Nanorods as an Efficient Catalyst for One-Pot Conversion of Nitrophenol/Nitroacetophenone into Benzoxazole/Quinazoline. *J. Am. Chem. Soc.* **2017**, *139* (16), 5712−5715.
(28) Yu, C.; Guo, X.; Yin, Z.; Zhao, Z.; Li, X.; Robinson, J.; Muzzio, M.; Castilho, C. J.; Shen, M.; Yuan, Y.; Wang, J.; Antolik, J.; Lu, G.; Su, D.; Chen, O.; Guduru, P.; Seto, C. T.; Sun, S. Highly Efficient AuPd Catalyst for Synthesizing Polybenzoxazole with Controlled Polymerization. *Matter* **2019**, *1* (6), 1631−1643.
(29) Hu, X.-D.; Jenkins, S. E.; Min, B. G.; Polk, M. B.; Kumar, S. Rigid-Rod Polymers: Synthesis, Processing, Simulation, Structure, and Properties. *Macromol. Mater. Eng.* **2003**, *288* (11), 823−843.
(30) Afshari, M.; Sikkema, D. J.; Lee, K.; Bogle, M. High Performance Fibers Based on Rigid and Flexible Polymers. *Polym. Rev.* **2008**, *48* (2), 230−274.
(31) Li, G. High-performance rigid-rod polymer fibers. In *Structure and Properties of High-Performance Fibers*; Bhat, G., Ed.; Elsevier BV: 2017; pp 141−166.
(32) Metin, Ö.; Sun, X.; Sun, S. Monodisperse Gold−Palladium Alloy Nanoparticles and Their Composition-Controlled Catalysis in Formic Acid Dehydrogenation under Mild Conditions. *Nanoscale* **2013**, *5* (3), 910−912.
(33) Zhu, W.; Michalsky, R.; Metin, Ö.; Lv, H.; Guo, S.; Wright, C. J.; Sun, X.; Peterson, A. A.; Sun, S. Monodisperse Au Nanoparticles for Selective Electrocatalytic Reduction of CO_2 to CO. *J. Am. Chem. Soc.* **2013**, *135* (45), 16833−16836.
(34) Mazumder, V.; Sun, S. Oleylamine-Mediated Synthesis of Pd Nanoparticles for Catalytic Formic Acid Oxidation. *J. Am. Chem. Soc.* **2009**, *131* (13), 4588−4589.
(35) Procházková, D.; Zámostný, P.; Bejblová, M.; Červený, L.; Čejka, J. Hydrodeoxygenation of Aldehydes Catalyzed by Supported Palladium Catalysts. *Appl. Catal., A* **2007**, *332* (1), 56−64.
(36) Volkov, A.; Gustafson, K. P. J.; Tai, C.-W.; Verho, O.; Bäckvall, J.-E.; Adolfsson, H. Mild Deoxygenation of Aromatic Ketones and Aldehydes over Pd/C Using Polymethylhydrosiloxane as the Reducing Agent. *Angew. Chem., Int. Ed.* **2015**, *54* (17), 5122−5126.
(37) Wang, S.; Zhou, P.; Jiang, L.; Zhang, Z.; Deng, K.; Zhang, Y.; Zhao, Y.; Li, J.; Bottle, S.; Zhu, H. Selective Deoxygenation of Carbonyl Groups at Room Temperature and Atmospheric Hydrogen Pressure over Nitrogen-Doped Carbon Supported Pd Catalyst. *J. Catal.* **2018**, *368*, 207−216.
(38) Dong, Z.; Yuan, J.; Xiao, Y.; Mao, P.; Wang, W. Room Temperature Chemoselective Deoxygenation of Aromatic Ketones and Aldehydes Pomoted by a Tandem Pd/TiO_2 + $FeCl_3$ catalyst. *J. Org. Chem.* **2018**, *83* (18), 11067−11073.
(39) Wolfe, J. F.; Arnold, F. E. Rigid-Rod Polymers. 1. Synthesis and Thermal Properties of Para-Aromatic Polymers with 2,6-Benzobisoxazole Units in the Main Chain. *Macromolecules* **1981**, *14*, 909−915.
(40) Maruyama, Y.; Oishi, Y.; Kakimoto, M.; Imai, Y. Synthesis and Properties of Fluorine-Containing Aromatic Polybenzoxazoles from Bis(o-aminophenols) and Aromatic Diacid Chlorides by the Silylation method. *Macromolecules* **1988**, *21*, 2305−2309.
(41) Fukumaru, T.; Saegusa, Y.; Fujigaya, T.; Nakashima, N. Fabrication of Poly(p-Phenylenebenzobisoxazole) Film Using a

https://dx.doi.org/10.1021/jacs.0c12488
J. Am. Chem. Soc. 2021, 143, 2115−2122

Soluble Poly(o-Alkoxyphenylamide) as the Precursor. *Macromolecules* **2014**, *47* (6), 2088−2095.
(42) Walsh, P. J.; Hu, X.; Cunniff, P.; Lesser, A. J. Environmental Effects on Poly-p-Phenylenebenzobisoxazole Fibers. I. Mechanisms of degradation. *J. Appl. Polym. Sci.* **2006**, *102* (4), 3517−3525.
(43) Park, E. S.; Sieber, J.; Guttman, C.; Rice, K.; Flynn, K.; Watson, S.; Holmes, G. Methodology for Detecting Residual Phosphoric Acid in Polybenzoxazole Fibers. *Anal. Chem.* **2009**, *81* (23), 9607−9617.
(44) Kanbargi, N.; Hu, W.; Lesser, A. J. Degradation Mechanism of Poly(p-Phenylene-2,6-Benzobisoxazole) Fibers by ^{31}P Solid-State NMR. *Polym. Degrad. Stab.* **2017**, *136*, 131−138.

https://dx.doi.org/10.1021/jacs.0c12488
J. Am. Chem. Soc. 2021, 143, 2115−2122